Electronic Supplementary Material (ESI) for Inorganic Chemistry Frontiers.

Supporting Information for

High spin polarized Fe_2 cluster combined with vicinal nonmetallic sites for catalytic ammonia synthesis by a theoretical perspective

Hongdan Zhu, [a] Jolyon Aarons, [b] Qian Peng, [a,] *

a State Key Laboratory and Institute of Elemento-Organic Chemistry and Frontiers Science Center for New Organic Matter, College of Chemistry, Nankai University, Tianjin 300071, China.

b Key Laboratory of Advanced Energy Materials Chemistry (Ministry of Education), College of Chemistry, Nankai University, Tianjin, 300071, China.

Dedicated to the 100th anniversary of Chemistry at Nankai University.

* *Email: qpeng@nankai.edu.cn.*

Table of Contents

1. Free energy calculation

For adsorbed molecules, their translational and rotational freedoms are restricted. Thus, the contribution of translation and rotation to entropy and enthalpy will be significantly reduced. Generally, we consider that this part of the contribution is transformed into vibrational energy and all 3N vibrations of adsorbed molecules are used to calculate the correction of thermodynamic quantities. Therefore, when calculating the Gibbs free energy of the adsorbed molecules, the thermodynamic contribution generated by the vibration freedom will be mainly considered.

Taking the bottom of the potential energy well as the zero point, the vibration partition function under the resonance approximation can be expressed as:

$$q_{vir} = \prod_i \frac{e^{-hv_i/2kT}}{1 - e^{-hv_i/kT}} \qquad \text{(eq-S1)}$$

Where q_{vir}, v_i, h and k represent vibration partition function, vibration frequency, Planck constant and Boltzmann constant, respectively.

So, the corrections of internal energy ($U_{vir}(T)$) and entropy ($S_{vir}(T)$) at a certain temperature can obtain by equation eq-S2 and eq-S3:

$$U_{vir}(T) = R\sum_i \left(\frac{hv_i}{k}\right)\left(\frac{1}{2} + \frac{e^{-hv_i/kT}}{1 - e^{-hv_i/kT}}\right) \qquad \text{(eq-S2)}$$

$$S_{vir}(T) = R\sum_i \left\{\frac{hv_i}{k}\frac{e^{-hv_i/kT}}{1 - e^{-hv_i/kT}} - \ln\left[1 - e^{-hv_i/kT}\right]\right\} \qquad \text{(eq-S3)}$$

And at 0 K, the zero-point vibrational energy (ZPE) of adsorbed molecules is:

$$ZPE = \frac{1}{2}\sum_i hv_i \qquad \text{(eq-S4)}$$

After vibrational frequency analysis, we can directly obtain the thermodynamic contribution and to calculate the corresponding Gibbs free energies at standard pressure and a certain temperature through VASPKIT code, a post-processing tool for VASP code [1].

Different from adsorbed molecules, for gas molecules, the calculation of Gibbs free energy needs to consider the contributions of translational energy, rotational energy and vibrational energy at the same time, which increases the complexity of the calculation.

Under 0 K, there is:

$$U(0) = \varepsilon_{ele} + ZPE \quad \text{(eq-S5)}$$

$$G(0) = H(0) = U(0) = \varepsilon_{ele} + ZPE \quad \text{(eq-S6)}$$

Here, We can obtain the enthalpy and entropy at a certain temperature and standard pressure in the NIST-JANAF thermodynamics table. So, the Gibbs free energy at standard pressure can be calculated as:

$$G(T,p^0) = G(0,p^0) + \Delta G_{0\to T} = \varepsilon_{ele} + ZPE + (\Delta H_{0\to T} - T\Delta S_{0\to T}) \quad \text{(eq-S7)}$$

According to the the ideal gas equation of state, the Gibbs free energy at certain temperature and pressure can be obtained as:

$$G(T,p) = G(T,p^0) + RT\ln p/p^0 \quad \text{(eq-S8)}$$

The zero-point vibrational energy and entropy corrections of gas molecules and adsorbted intermediate species involved in N_2-to-NH_3 conversion at standard condition (T = 298.15 K and p^0 = 1 bar) are listed in Table S1.

Table S1. Free energy corrections for gas molecules and adsorbted intermediate species.

Species	*ZPE* (eV)	*TS* (eV)	*ZPE-TS* (eV)
N_2	0.15	0.57	-0.42
H_2	0.27	0.39	-0.12
NH_3	0.91	0.58	0.33
N_2*	0.20	0.09	0.11
N_2*+4H*	1.49	0.11	1.38
N_2*（B/g-C_3N_4）	0.20	0.09	0.11
N_2*+4H* (B/g-C_3N_4)	1.43	0.11	1.32

2. Microkinetic analysis

Microkinetic analysis of Fe_2/mpg-C_3N_4 and Fe_2/B/mpg-C_3N_4 by the Energetic Span model, proposed by Kozuch *et al* [2], are conducted to further probe the reaction rate for the influence of B doping and the

catalytic performance. This theoretical model proposes that aside from the rate-limiting step, the steps before and after it also have impacts on the *TOF*, and thus the apparent activation energy rather than the activation energy of a single rate-limiting step can determine the whole reaction activity. In this model, the *TOF*-determining transition state (TDTS) and *TOF*-determining intermediate (TDI) are used to identify the apparent activation energy (δG_a) following Equation (eq-S9):

$$\delta G_a = \begin{Bmatrix} T_{TDTS} - I_{TDI} & if\ TDTS\ appears\ after\ TDI \\ T_{TDTS} - I_{TDI} + \Delta G_r & if\ TDTS\ appears\ before\ TDI \end{Bmatrix} \quad \text{(eq-S9)}$$

Where, the TDTS and the TDI are the TS and the intermediate that maximize the energetic span within the cyclic constraints, and thereby gauge the kinetics of the cycle.

The TOF can be calculated following Equation (eq-S10)

$$TOF = \frac{k_B T}{h} e^{-\delta G_a / k_B T} \quad \text{(eq-S10)}$$

Because of the condition that the TDI and TDTS must be the ones that maximize the energetic span, the determining states may be different from the extreme state of the energy graph. According to the reaction free energy diagrams from Fe_2/mpg-C_3N_4 and Fe_2/B/mpg-C_3N_4,(Fig.S18 and Fig.S24):

$$TS(\text{a3-a4}) - I(a12) + \Delta G_r > TS(a1 - a2) - I(*N_2) \quad \text{(eq-S11)}$$

Thus, $T_{TDTS}\ and\ I_{TDI}$ are *TS*(a3-a4) and a12 respectively. In order to investigate the effect of different temperatures and pressures on the reaction rate, we plot a TOF map with pressure (1-100 bar) and temperature(300-700 K) of ammonia synthesis on Fe_2/B/mpg-C_3N_4(Fig. 7b). In addition, we also considered the impact of different partial pressures on TOF (Fig. 7c). In addition, we also tried to carry out the Microkinetic modeling by using the CatMAP Software package [3] but it seems not to be applicable in our mechanism probably because multiple adsorption sites would lead the Microkinetic model much too complex to be solved.

3. Results and Discussion

3.1. The vicinal nonmetallic sites-promoted Hydrogenation Mechanism

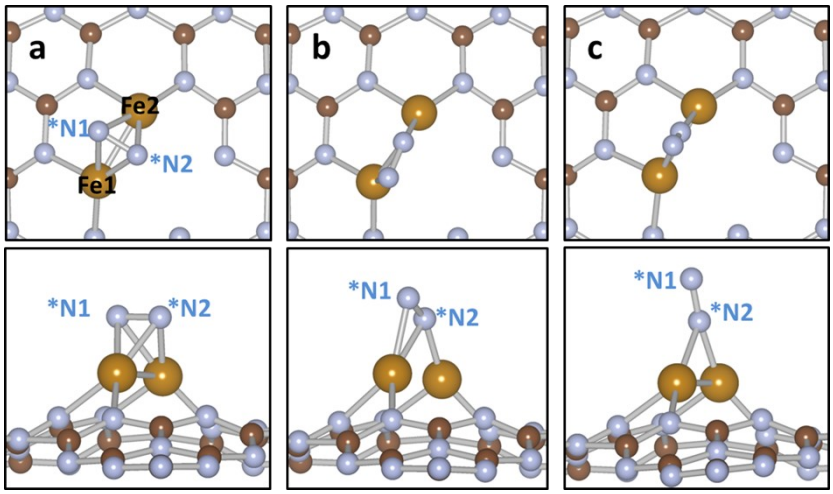

Fig. S1. Optimized configurations for N_2 adsorption on Fe_2/mpg-C_3N_4 (Gray: C, Silver: N, Golden; Fe).

Table S2. Structural properties of N_2 adsorption configurations on Fe_2/mpg-C_3N_4.

Adsorption Structures	Adsorption Model	E_{ads}/eV[a]	Magnetic Moment/μ	N-N bond Length/Å	Bader charge of N_2/|e|
a	μ-η2:η2	-1.52	4.13	1.25	-0.86
b	μ-η2:η1	-1.50	4.04	1.20	-0.72
c	η1: η1	-1.29	4.06	1.16	-0.56

[a] E_{ads} is the adsorption energy of the surface species, calculated according to eq-2.

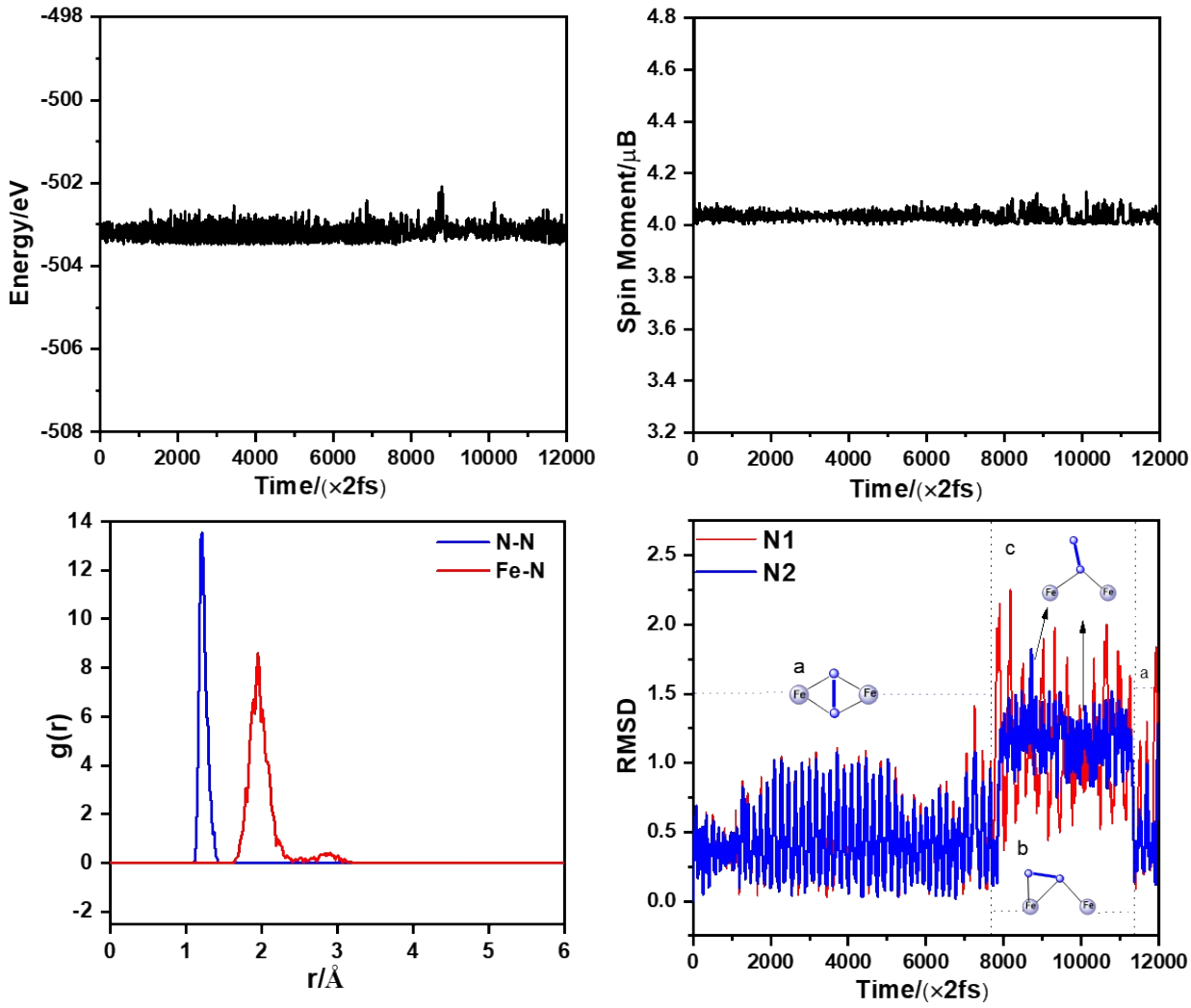

Fig. S2. AIMD simulations for on Fe_2/mpg-C_3N_4. (a) Fluctuations of potential energy with time; (b) Spin moment change with time. (c) Radial distribution functions (RDFs) of Fe-N and N-N in N_2 adsorption constructions; (d) Root-mean-square deviation (RMSD) of *N1 and *N_2 in N_2 （Structure a is mainly distributed before 7800($\times 2fs$), after that, there are mainly structure b and a small amount of structure c. Structure a appeared again after 11300($\times 2fs$).).

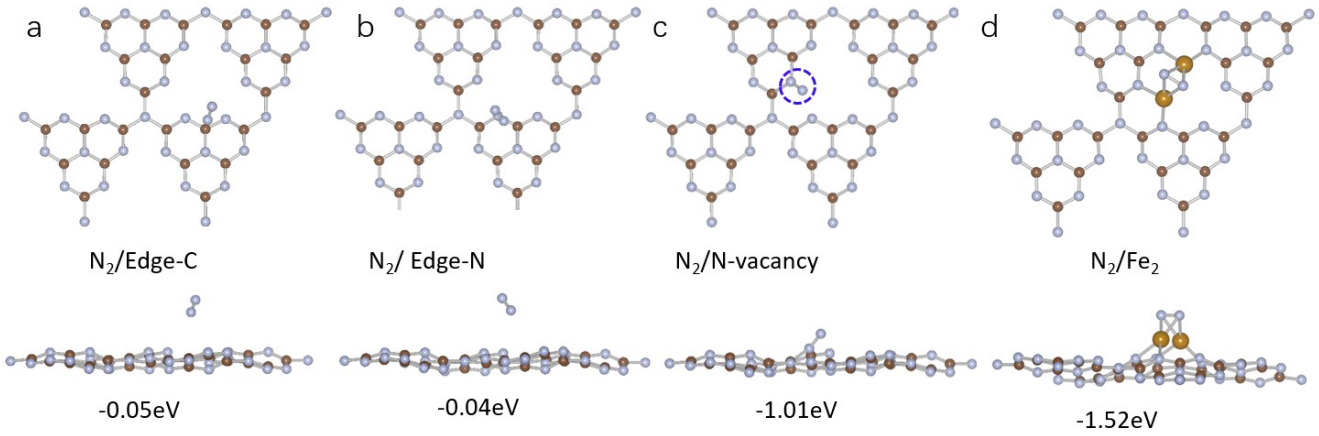

Fig. S3. Optimized structures for the adsorption of $*N_2$ on C_3N_4 and N-vacancy of C_3N_4.

We have considered the adsorption of nitrogen on C_3N_4. As seen in Fig. S3, calculated results indicating that the C_3N_4 cannot effectively stabilize and activate N_2 (Fig. s3a-b). In comparison, N-vacancy (Fig. S3c) can adsorb and activate N_2, which was is confirmed by recent literature[4]. However, the adsorption energy on the Fe_2 site (Fig. S3d) is 0.51 eV more stable than that on N-vacancy. Therefore, Fe_2 with high spin polarization is more favorable for activating nitrogen in our model.

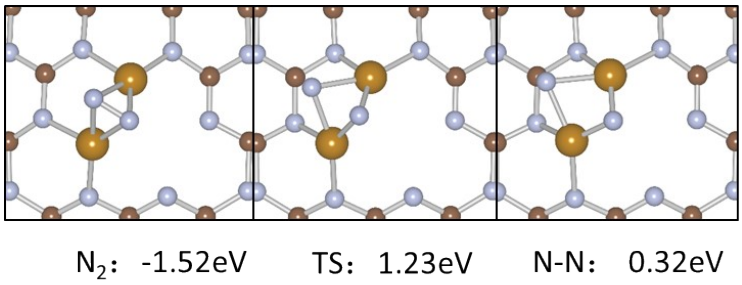

Fig. S4. Optimized configurations for N_2 dissociation on Fe_2/mpg-C_3N_4 (Pink: H, Gray: C, Silver: N, Golden: Fe).

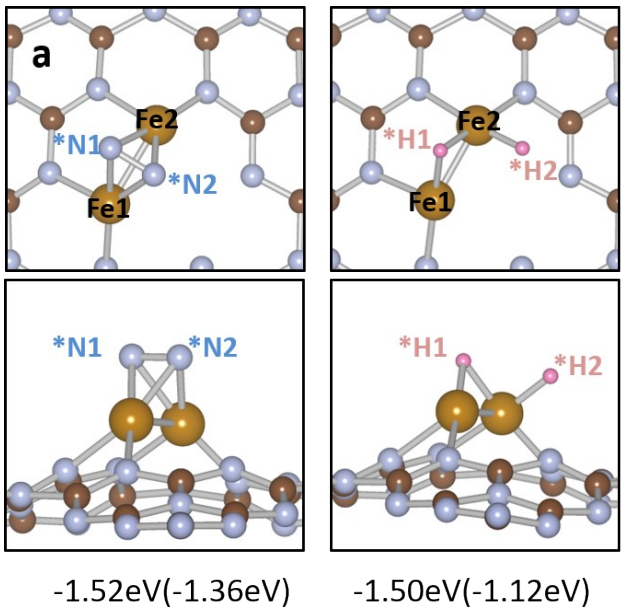

Fig. S5. Optimized adsorption configurations and Gibbs free energies for N_2 and H_2 on Fe_2 cluster. (Pink: H, Gray: C, Silver: N, Golden: Fe).

When considering the adsorption of reactants, we consider the adsorption of H_2 on Fe_2 cluster. As shown in Fig.S5, calculated results show that Nitrogen adsorption is more stable than hydrogen adsorption, especially the Gibbs free energy of nitrogen is 0.24eV more stable than hydrogen.

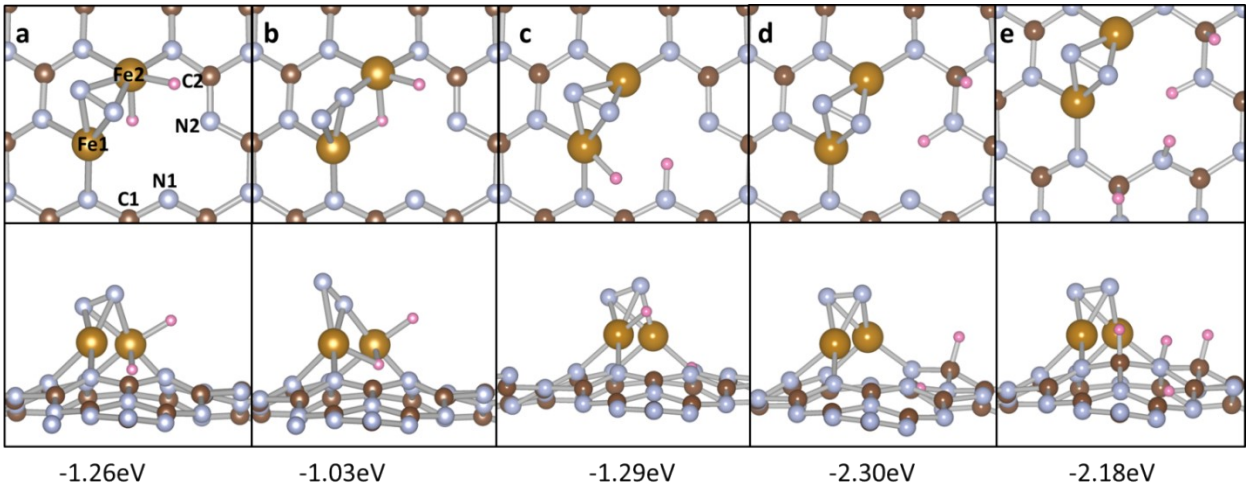

Fig. S6. Optimized configurations for N_2 and H_2 adsorption simultaneously on Fe_2/mpg-C_3N_4 (Pink: H, Gray: C, Silver: N, Golden: Fe).

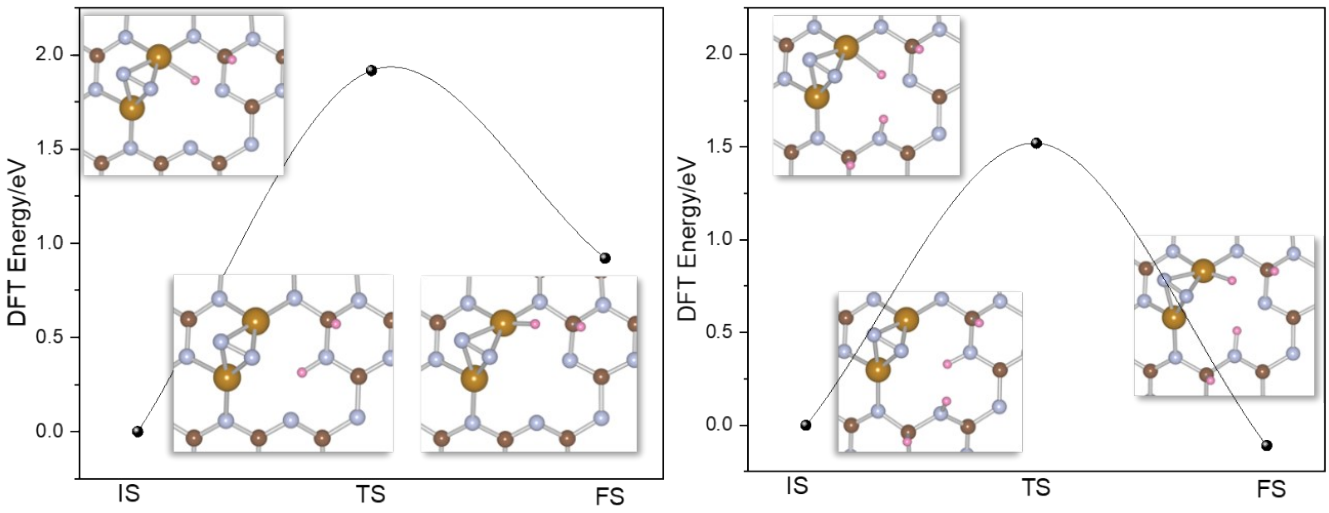

Fig. S7. Hydrogen transfer processes in the N sites on Fe_2/mpg-C_3N_4 (Pink: H, Gray: C, Silver: N, Golden: Fe).

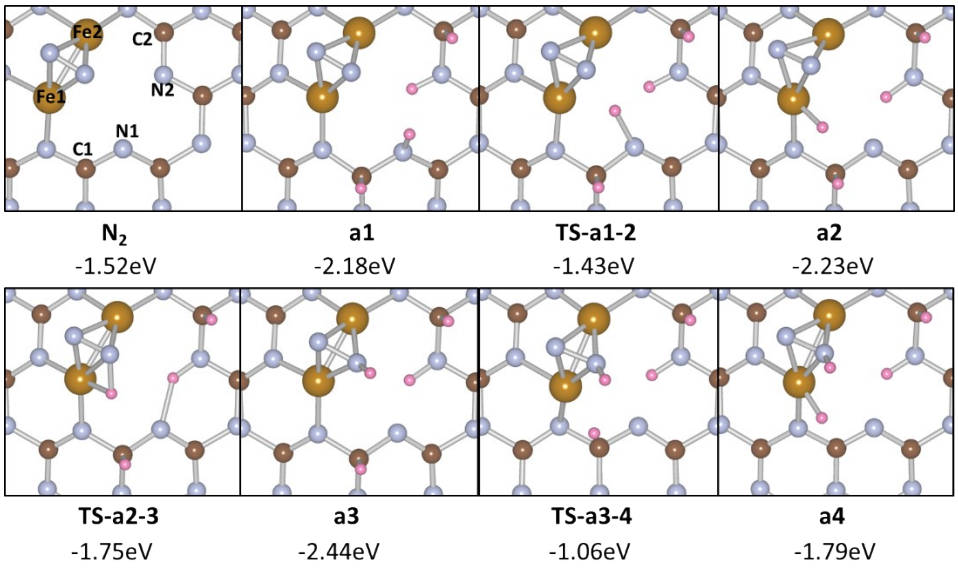

Fig. S8. Structures of the Hydrogen transfer process on Fe_2/mpg-C_3N_4 (Pink: H, Gray: C, Silver: N, Golden: Fe).

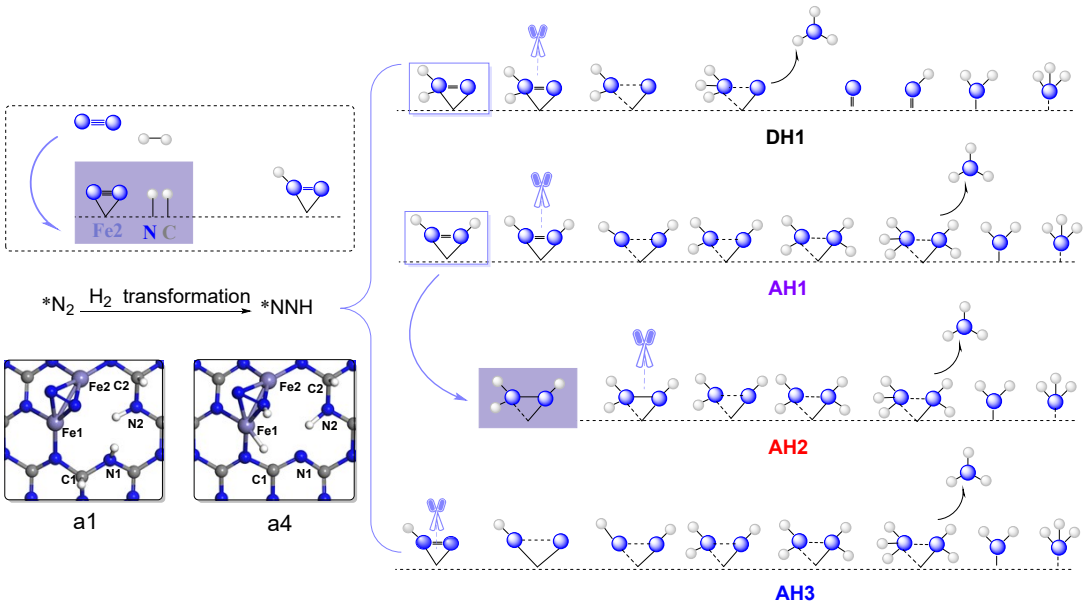

Fig. S9. Schematic depiction of four different association mechanisms for the thermal conversion of N_2 to NH_3 on Fe_2/mpg-C_3N_4. (AH and DH are abbreviations for Alternative and Distal Hydrogenation, respectively. The inset structures represent the co-adsorption configuration of N_2+2H_2 and *NNH intermediate (a2 and a5 in Fig. 2)

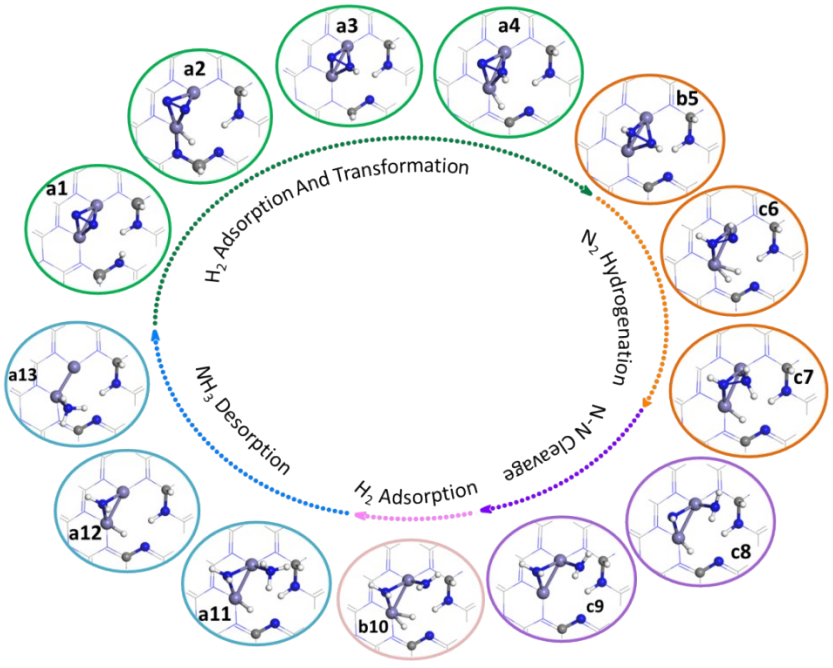

Fig. S10. Preferred reaction pathway for the thermal conversion of N_2 to NH_3 on Fe_2/mpg-C_3N_4.

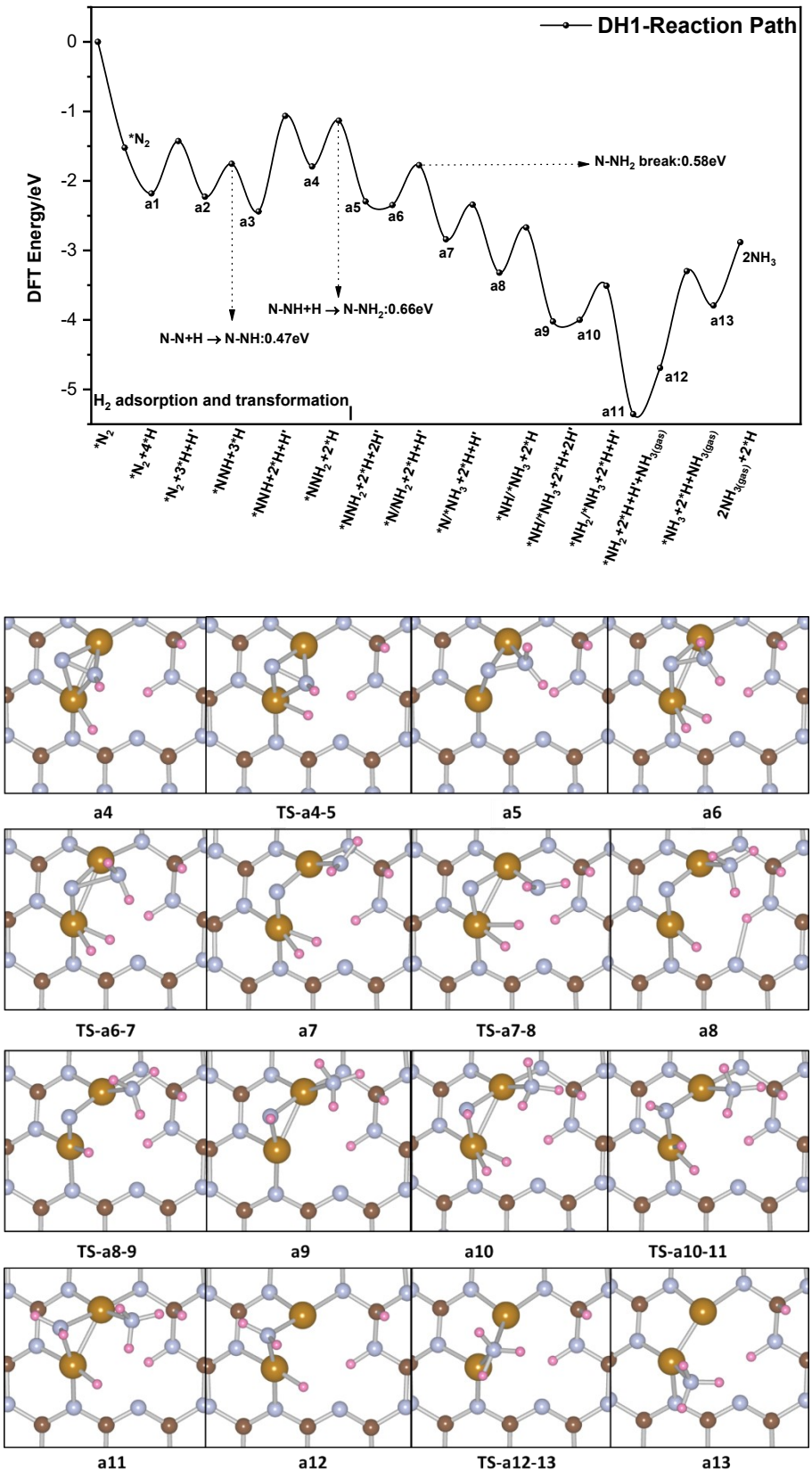

Fig. S11. Energy profile and structures of the surface species for the distal hydrogenation (DH1) of N_2 on Fe_2/mpg-C_3N_4 (Pink: H, Gray: C, Silver: N, Golden; Fe).

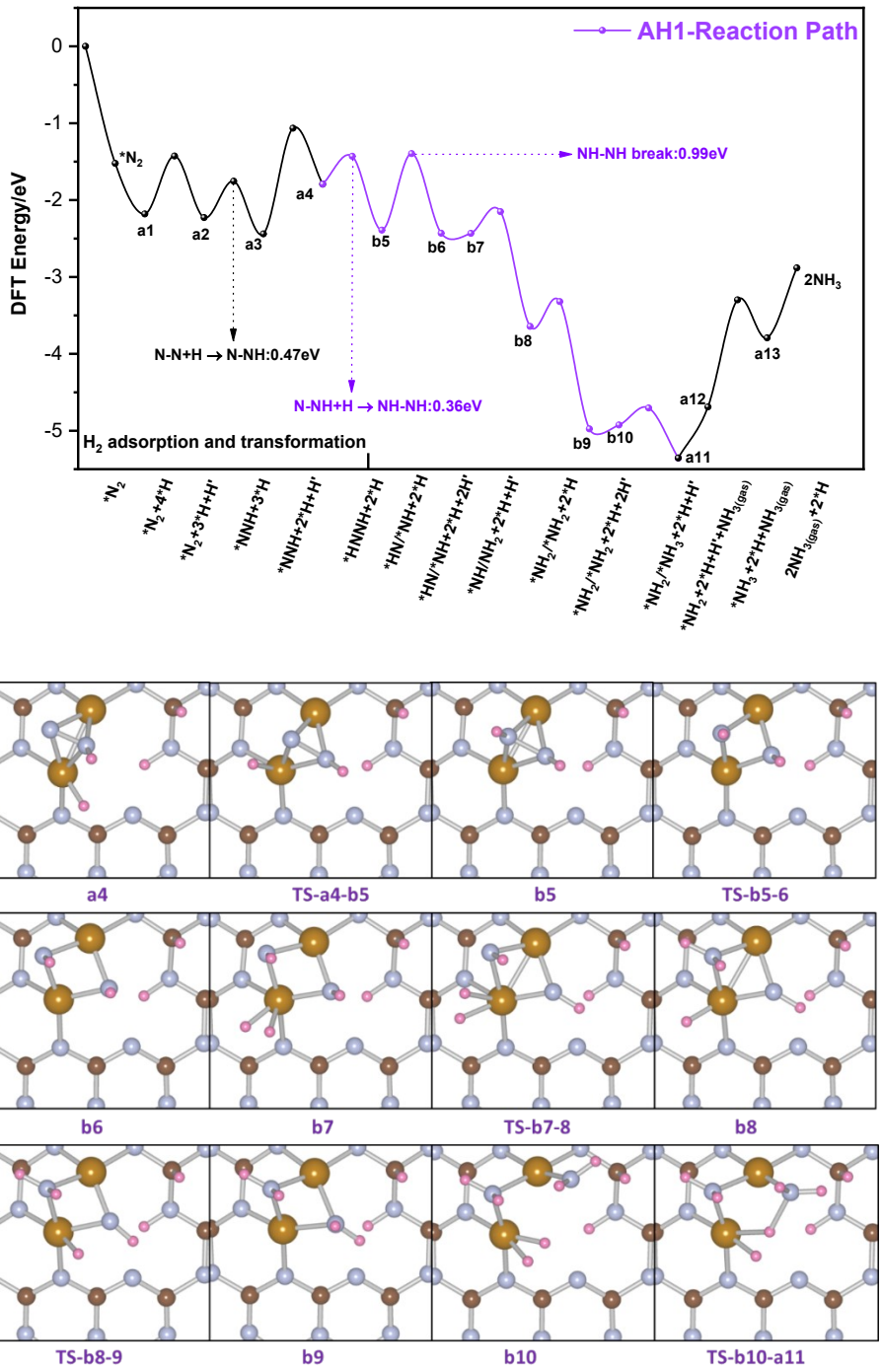

Fig. S12. Energy profile and structures of the surface species for the alternative hydrogenation (AH1) of N_2 on Fe_2/mpg-C_3N_4 (Pink: H, Gray: C, Silver: N, Golden; Fe).

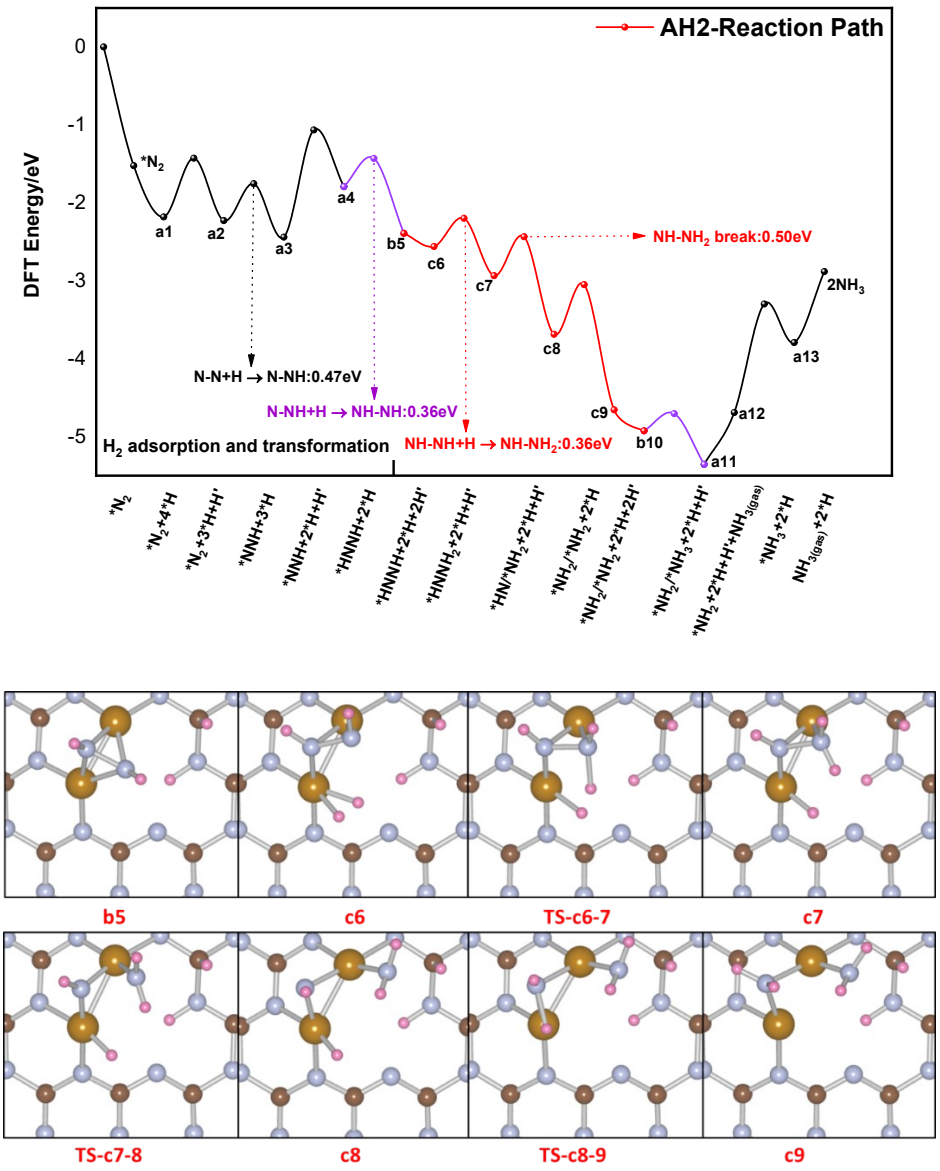

Fig. S13. Energy profile and structures of the surface species for the alternative hydrogenation (AH2) of N_2 on Fe_2/mpg-C_3N_4 (Pink: H, Gray: C, Silver: N, Golden; Fe).

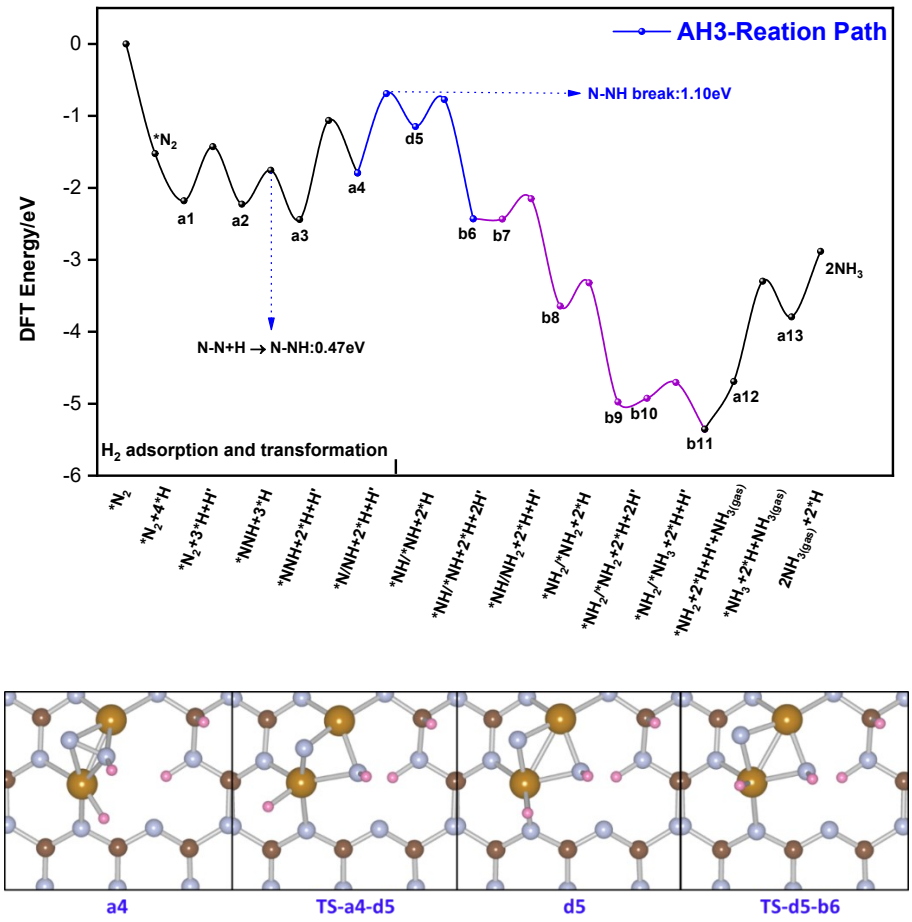

Fig. S14. Energy profile and structures of the surface species for the alternative hydrogenation (AH3) of N_2 on Fe_2/mpg-C_3N_4 (Pink: H, Gray: C, Silver: N, Golden; Fe).

Table S3. N-N bonds and Bader charge of N_2 for NH_xNH_y(x=0-3, y=0-3) intermediates on Fe_2/mpg-C_3N_4.

NH_xNH_y Intermediates	Adsorption Structures [a]	N-N break Energy barriers/eV	N-N bond length/Å	Bader charge/|e|
N-NH	a5	1.10	1.33	-1.18
NH-NH	b6	0.99	1.40	-1.57
N-NH_2	a7	0.58	1.43	-1.48
NH-NH_2	c8	0.50	1.44	-1.60

[a] Adsorption Structures come from Fig. 2.

Table S4. Transition state energy barriers (eV) of several elementary reactions by use PBE functional and empirical dispersion correction (Grimme-D3) to PBE functional.

	PBE	PBE(D3)
TS-a1-2	0.75	0.79
TS-a2-3	0.47	0.47
TS-a3-4	1.38	1.40
TS-a4-b5	0.36	0.35
TS-c6-c7	0.36	0.32
TS-c7-c8	0.50	0.49

By comparing the transition state energy barriers of several elementary reactions in the optimal reaction pathway, we found that there will be a slight difference in energy when using the empirical dispersion correction (Grimme-D3) to PBE functional, but it will not affect the results of reaction mechanism.

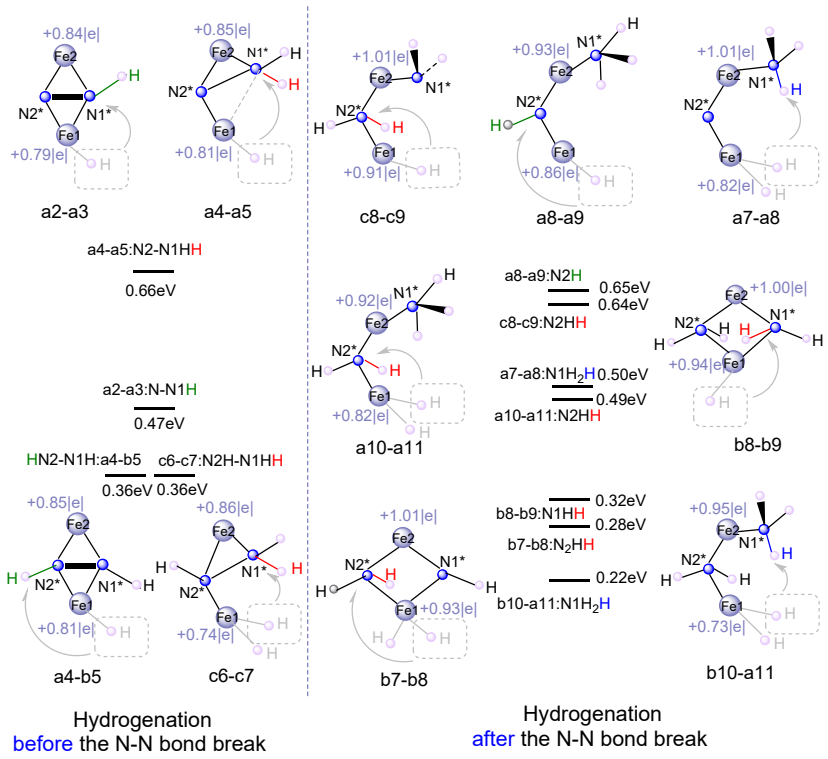

Fig. S15. N-H bond formation energy barriers in all hydrogenation mechanisms. (The hydrogen transferred on -N, -NH, and -NH_2 is labeled green, red and blue, respectively).

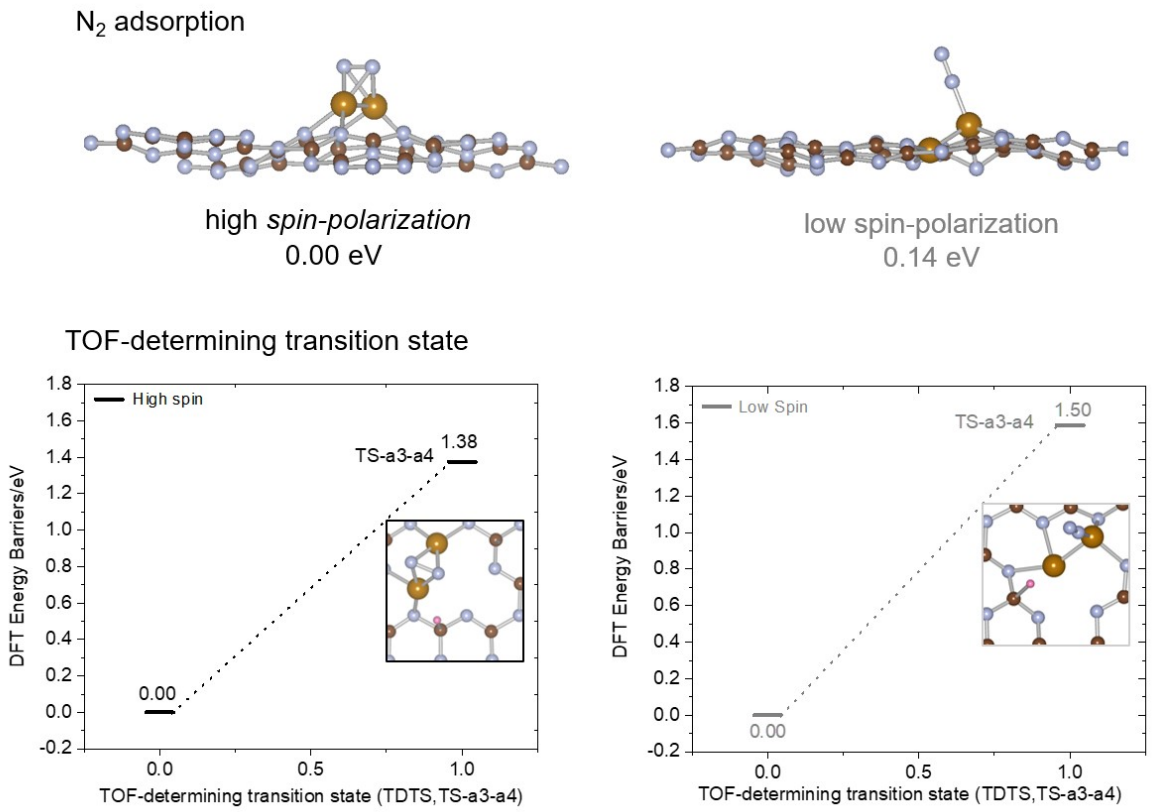

Fig. S16. Optimized N_2 adsorption structures and TOF-determining transition state on energy-degenerate Fe_2/mpg-C_3N_4 configurations. (Pink: H, Gray: C, Silver: N, Golden; Fe).

Indeed,we have indeed also found that there are two energy-degenerate configurations of Fe_2 on g-C_3N_4, exhibiting different spin-polarizations. However, In the thermal catalytic synthesis of ammonia, how to activate the inert nitrogen would be a key issue. Our calculation results show that high-spin polarized Fe_2 with stronger electron donating ability for $2\pi^*$ of N_2 is more beneficial to activate nitrogen based on N_2 adsorption (Fig. S16). In addition, the TOF-determining transition state (TDTS) (TS-a3-a4 in Fig. 3b of main text) on high-spin polarized Fe_2 is 0.12eV lower than that on low-spin polarized Fe_2, which would affect the reaction rate of the catalytic cycle. Thus, low-spin polarized Fe_2/mpg-C3N4 does not have a catalytic advantage in the thermal catalytic synthesis of ammonia.

3.2. Nitrogen Reduction Mechanisms on various Iron clusters

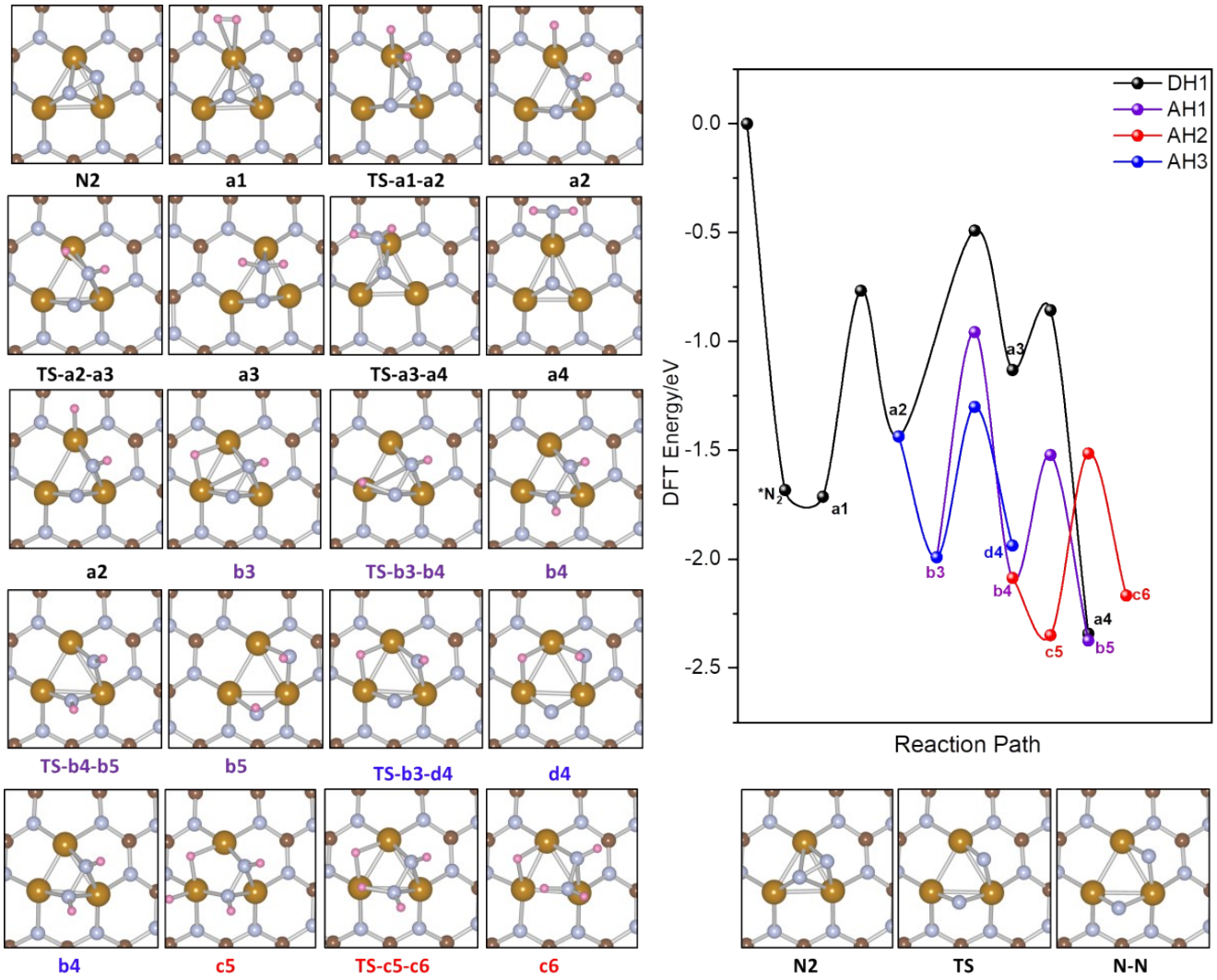

Fig. S17. Structures of the surface species and the energy profiles for the Nitrogen hydrogenation mechanisms on Fe_3/mpg-C_3N_4 (Pink: H, Gray: C, Silver: N, Golden; Fe).

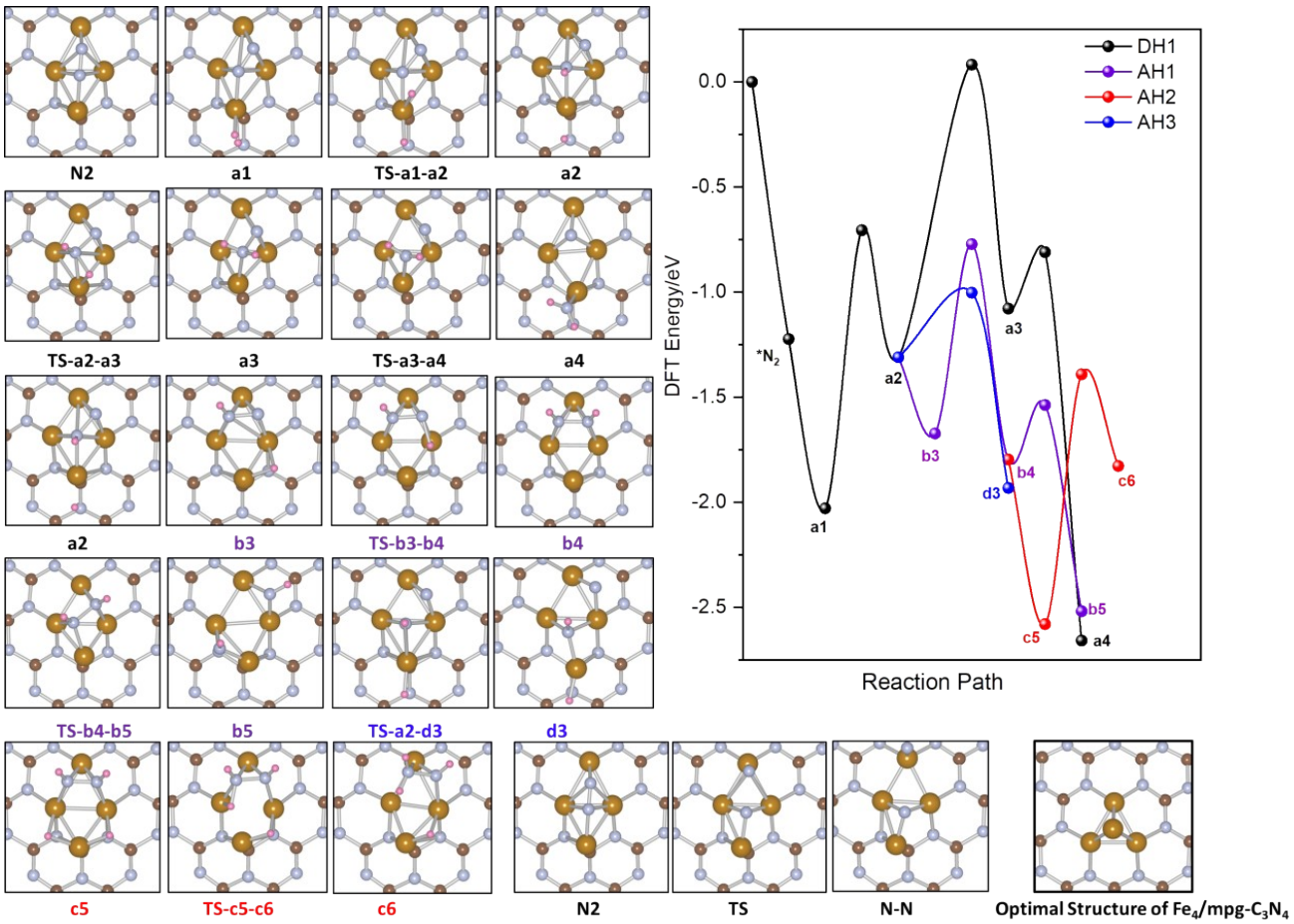

Fig. S18. Structures of the surface species and the energy profiles for the Nitrogen hydrogenation mechanisms on Fe_4/mpg-C_3N_4 (Pink: H, Gray: C, Silver: N, Golden; Fe). (Note that the Fe_4/g-C_3N_4 in this reaction pathway is not the most stable Fe_4 cluster, and we designed this structure only to study the effect of iron coordination numbers on the reaction mechanism).

3.3. Electronic structure analysis

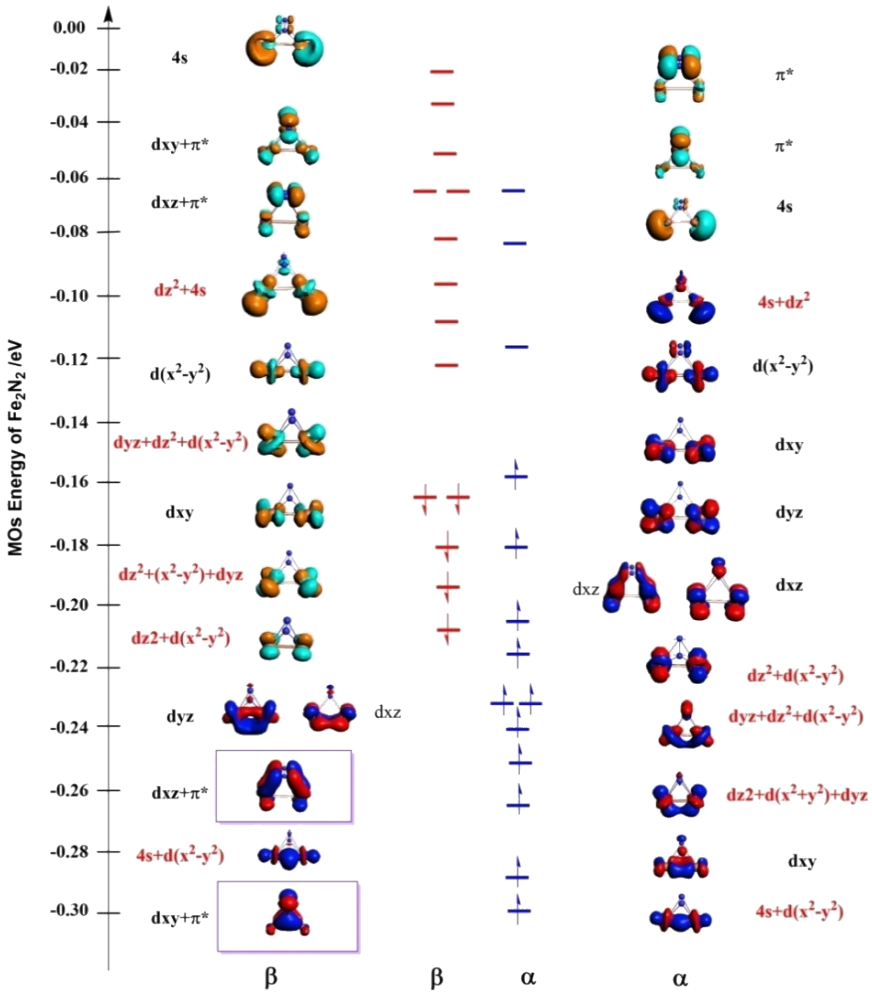

Fig. S19. MOs analysis of the Fe_2N_2 Simplified model with C_{2v} configuration based on SR-ZORA PBE/DZP calculations and the energy levels of Fe_2 α-orbitals are much lower than those of the β-orbitals. (The components of the orbitals marked in red are mixed, and the former has the most orbital components)

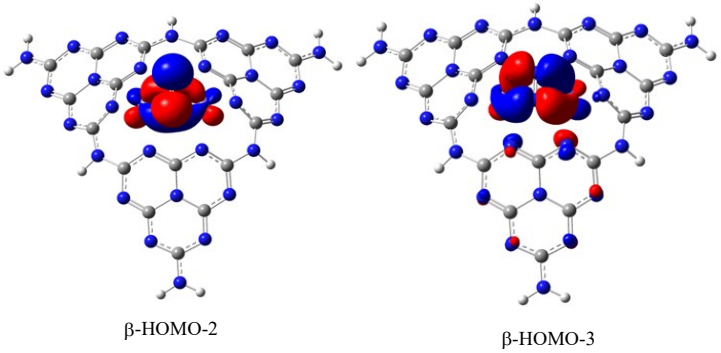

Fig. S20. Occupied partial molecular orbitals of the Nitrogen adsorption conformation on Fe_2/mpg-C_3N_4 based on wb97xd/def2svp calculations, the shape of orbitals is consistent with the bond orbitals between nitrogen and simplified model Fe_2 cluster (Fig. S17).

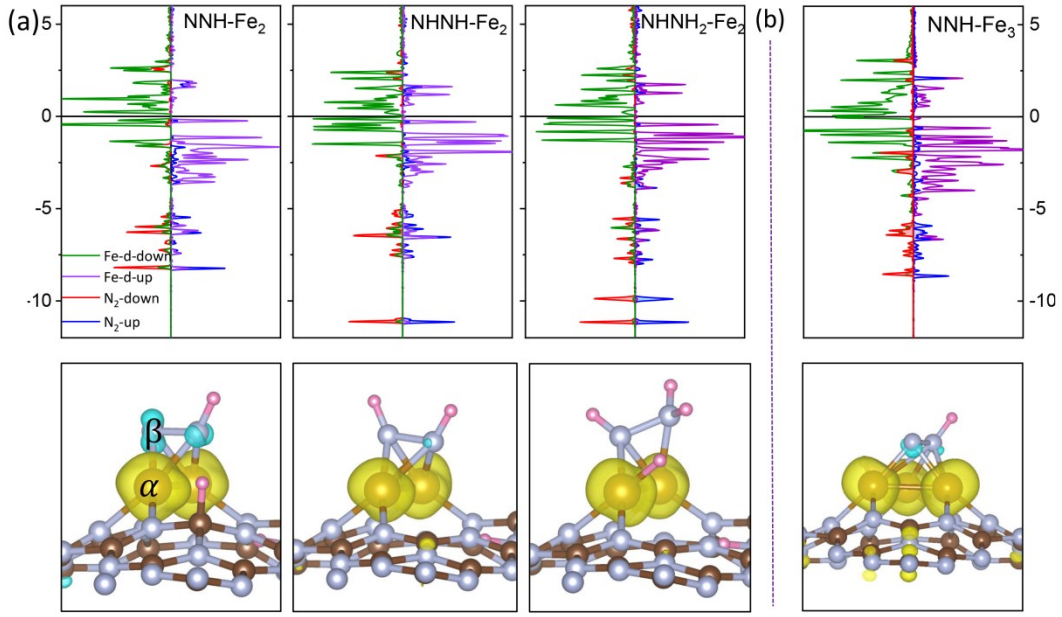

Fig. S21 (a) Projected electronic density of states (PDOS) of NH_xNH_y species and corresponding spin densities in Fe_2/mpg-C_3N_4; (b) Projected electronic density and spin density of *NNH in Fe_3/mpg-C_3N_4.

To understand the unusual hydrogenation mechanism of N_2 on the Fe_2/mpg-C_3N_4, projected density of states (PDOS) and spin densities for key intermediates were shown in Fig.S20. With continuous hydrogenation, both Fe_2 clusters and absorbed hydrogens transfer their electrons to N_2 2π* orbitals, which decreased the energy of the N-N anti-bond orbital and activates the N-N bond in Fig. 6a. The formed *NNH has relatively high spin polarization to make the next hydrogenation favorable, forming *NHNH via an alternate pathway. Because α-spin electrons of N_2 2π*orbitals keep increasing from *NN to *$NHNH_2$, the spin density for each intermediate is gradually eroded. After that, the following transformation would favor the dissociation of the N-N bond rather than additional hydrogenation. In contrast, the spin density of *NNH in Fe_3/g-C_3N_4 (Fig. 6b) is relatively low comparing with that in Fe_2/g-C_3N_4, and thus continuous hydrogenation was hindered.

3.4. The efficient catalyst by B doping mpg-C_3N_4

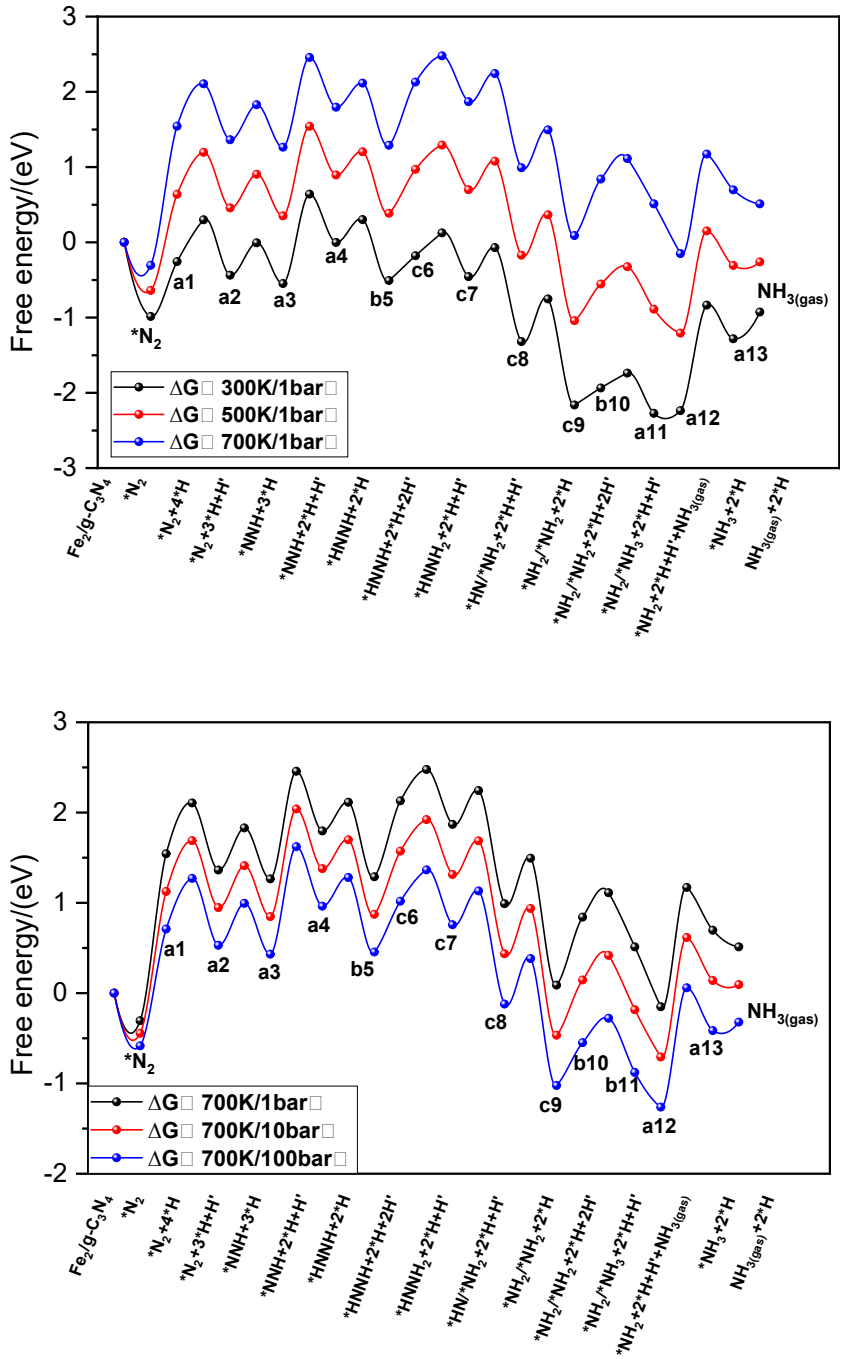

Fig. S22. Gibbs free energy diagram for ammonia synthesis on the Fe_2/mpg-C_3N_4. Reaction conditions and parameters are: H_2:N_2 ratio = 3:1 and NH_3 conversion is fixed at 10 %.

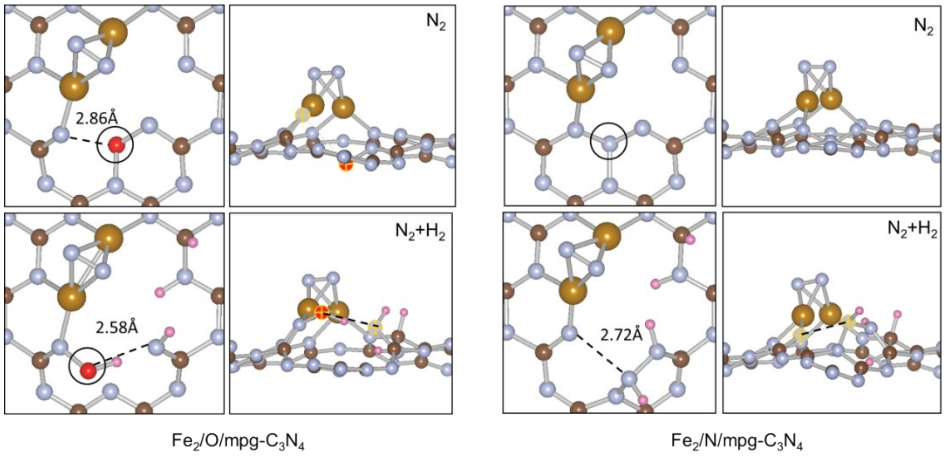

Fig. S23. Optimized N_2 adsorption configurations and co-adsorptions of N_2 and H_2 on O / N doped Fe_2/mpg-C_3N_4 (Fe_2/O/mpg-C_3N_4 and Fe_2/N/mpg-C_3N_4), respectively (Pink: H, Gray: C, Silver: N, red: O, Golden; Fe).

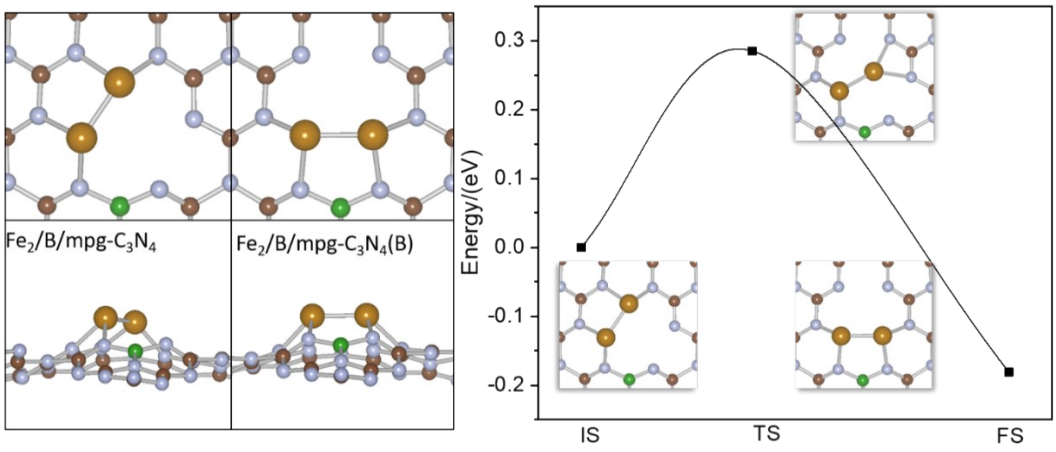

Fig. S24. Atomic configurations for Fe_2 dimers on the B doped mpg-C_3N_4 and the transformation of the two configurations, including IS, TS, and FS.

As seen in Fig. S23-S25, although the other Fe_2/B/mpg-C_3N_4(B), is slightly stable in thermodynamics (ΔE=-0.18eV), it is easy to transform into the Fe_2/B/mpg-C_3N_4 in main text with kinetics barrier (E_a=0.29 eV). And the most stable adsorption energy of nitrogen for these two configurations is similar. When considering the co-adsorption of nitrogen and hydrogen, the B-N site of Fe_2/B/mpg-C_3N_4(B) configuration becomes unfavorable for the adsorption and activation of hydrogen (around 1.1 eV, see b/b'and c/c' in Fig. S24). Therefore, the Fe_2/B/mpg-C_3N_4 in main text is stable with proper Fe_2 binding for the efficient hydrogen transfer.

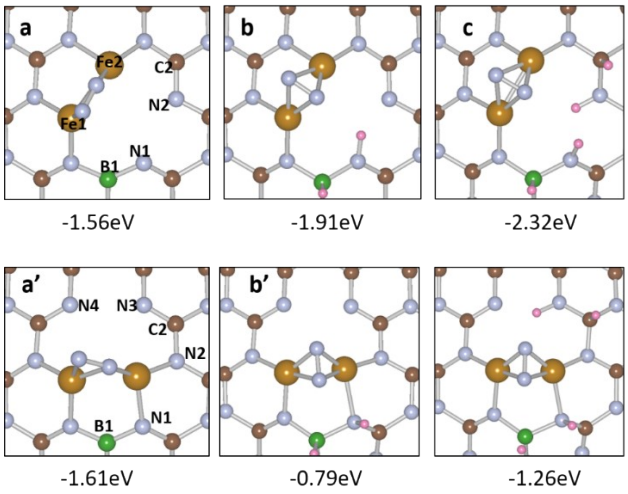

Fig. S25. Optimized N_2 adsorption configurations and co-adsorptions of N_2 and H_2 on B doped Fe_2/mpg-C_3N_4, (Pink: H, Gray: C, Silver: N, green: B, Golden; Fe).

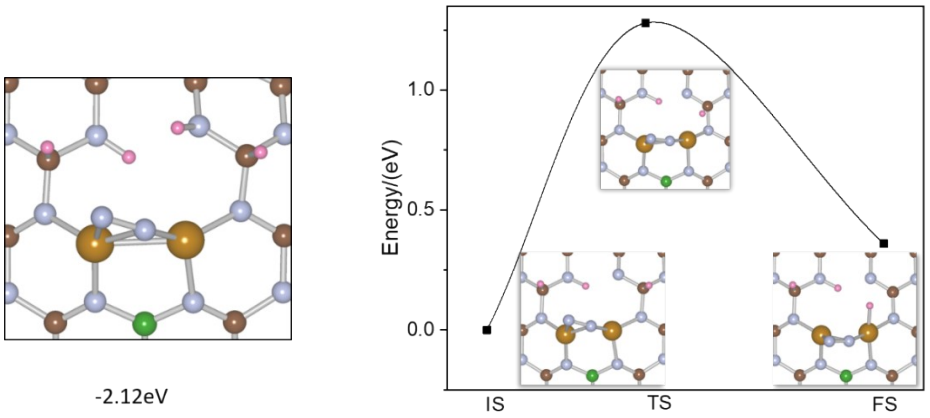

Fig. S26. Most co-adsorption configuration and hydrogen transfer processes in the C site on B doped Fe_2/mpg-C_3N_4 (Fe_2/B/mpg-C_3N_4(B)), (Pink: H, Gray: C, Silver: N, green: B, Golden; Fe).

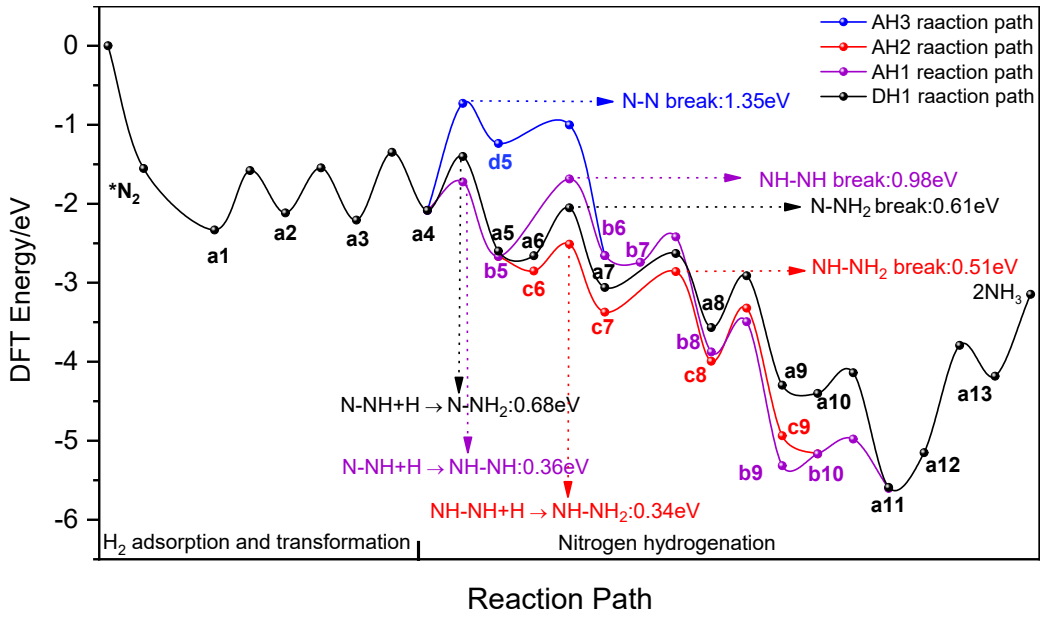

Fig. S27. Energy diagrams of four different association mechanisms for conversion of N_2 to NH_3 catalyzed by Fe_2/B/mpg-C_3N_4.

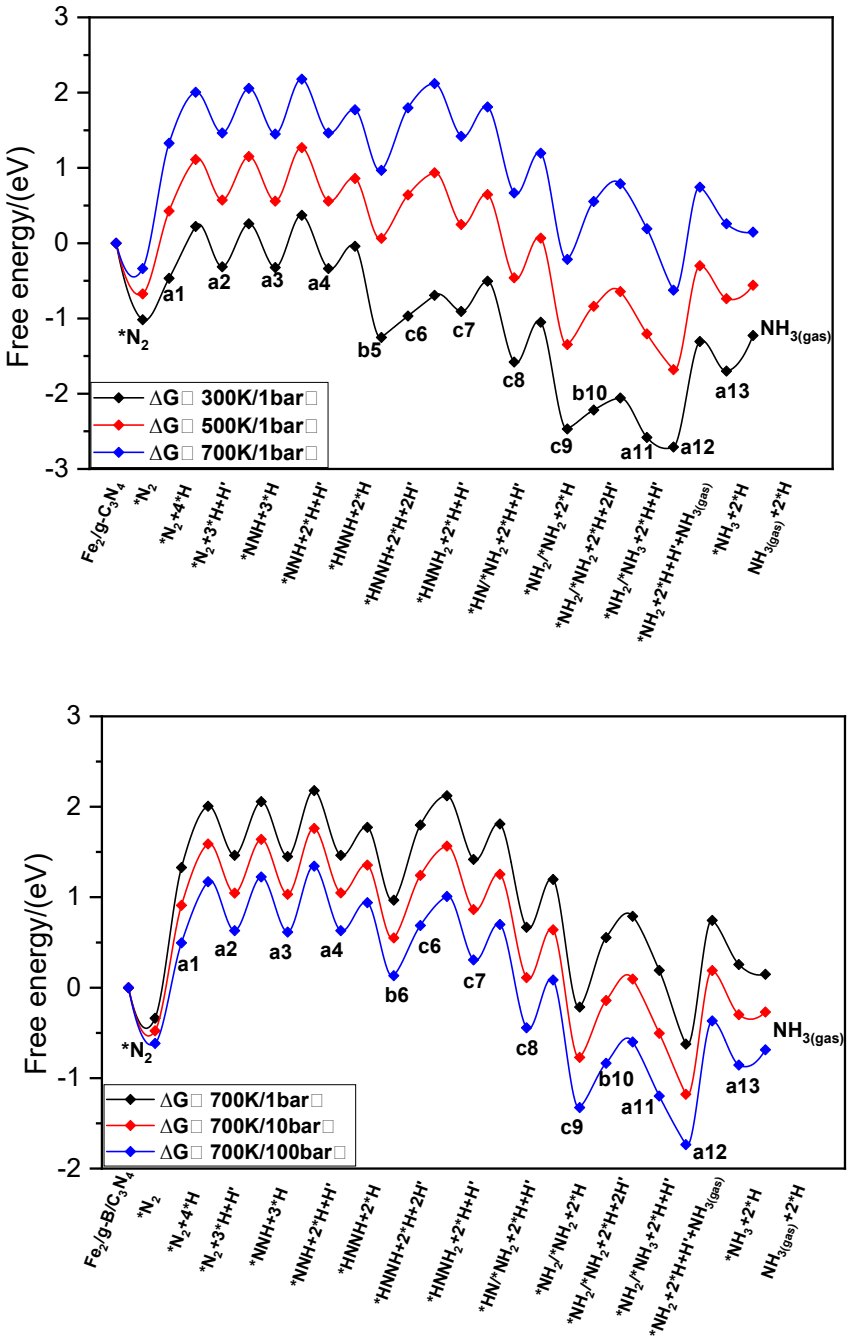

Fig. S28. Gibbs free energy diagram for ammonia synthesis on the Fe_2/B/mpg-C_3N_4. Reaction conditions and parameters are: H_2:N_2 ratio = 3:1 and NH_3 conversion is fixed at 10 %.

References

1 V. Wang, N. Xu, J. C. Liu, G. Tang, W. T. Geng, VASPKIT: A user-friendly interface facilitating high-throughput computing and analysis using VASP code, *Comput. Phys. Commun.* 2021, **267** 108033.

2 K. Sebastian, S. Sason, How to Conceptualize Catalytic Cycles? The Energetic Span Model, *Acc. Chem. Res.* 2011, **44** 101-110.

3 A. J. Medford, C. Shi, M. J. Hoffmann, A. C. Lausche, S. R. Fitzgibbon, T. Bligaard and J. K. Nørskov, CatMAP: A Software Package for Descriptor-Based Microkinetic Mapping of Catalytic Trends, *Catal. Lett.* 2015, **145** 794-807.

4 Z. Zhao, Y. Long, S. Luo, Y. Luo, M. Chen, J. Ma, Metal-Free C_3N_4 with plentiful nitrogen vacancy and increased

specific surface area for electrocatalytic nitrogen reduction, *J. Energy Chem.* 2021, **60** 546-555.